Research Article

Microstructure and mechanical properties of *h*-BN/Yb$_4$Si$_2$O$_7$N$_2$ composites

Juanjuan CHEN^{a,b}, Jixin CHEN^{a,*}, Hao ZHANG^{a,c}, Minmin HU^{a,c}, Meishuan LI^{a}

^{a}*Shenyang National Laboratory for Materials Science, Institute of Metal Research,*
Chinese Academy of Sciences, Shenyang, China
^{b}*University of Chinese Academy of Sciences, Beijing, China*
^{c}*School of Materials Science and Engineering, University of Science and Technology of China, Shenyang, China*

Abstract: A series of *h*-BN based composites with Yb$_4$Si$_2$O$_7$N$_2$ as a secondary phase were successfully synthesized by an *in situ* reaction hot pressing method. It was found that the relative density and room-temperature mechanical properties monotonically increased with increasing the content of Yb$_4$Si$_2$O$_7$N$_2$ from 20 to 50 vol%. When 50 vol% Yb$_4$Si$_2$O$_7$N$_2$ was introduced, the relative density of the composite reached 98.75%, and its flexural strength, compressive strength, fracture toughness, and hardness reached 338±10 MPa, 803±49 MPa, 2.06±0.06 MPa·m$^{1/2}$, and 2.69±0.10 GPa, respectively. The strengthening effect of Yb$_4$Si$_2$O$_7$N$_2$ was mainly attributed to its high modulus and high hardness. Fine microstructure was also advantageous to strength and could lead to more tortuous crack propagation paths and then improve the fracture toughness of the composites simultaneously. Meanwhile, the composites maintained good machinability.

Keywords: *h*-BN/Yb$_4$Si$_2$O$_7$N$_2$ composites; microstructure; mechanical properties; machinability

1 Introduction

Hexagonal boron nitride (*h*-BN), a layered material similar to graphite, is well known as an important ceramic because of its unique properties, such as thermal stability, high thermal conductivity, good thermal shock resistance [1–6], reliable electrical insulation, chemical inertness, excellent machinability [7–11], etc. *h*-BN is also used to improve the thermal shock resistance, machinability, and electrical insulation of other ceramics [12–14]. However, *h*-BN has low intrinsic mechanical properties due to its special layered

structure and poor sinterability. For example, the flexural strength and compressive strength of pure *h*-BN ceramic are only 75.8 and 124.1 MPa, respectively [15]. It has been shown that the incorporation of a secondary phase is an effective way to enhance the mechanical properties of the *h*-BN matrix [16–20].

Trice and Halloran [16] introduced Y$_2$Si$_2$O$_7$ into *h*-BN and attained *h*-BN–Y$_2$Si$_2$O$_7$ composites. It was demonstrated that the flexural strength could be increased by increasing the content of additive. Similarly, the mechanical properties, especially at high temperatures, were improved by introducing Y$_2$SiO$_5$ phase to the *h*-BN matrix [19,20]. In addition to these, Y$_4$Si$_2$O$_7$N$_2$–BN composites were also studied [21]. When the content of Y$_4$Si$_2$O$_7$N$_2$ was 70 vol%, the flexural strength was as high as 280 MPa. However,

* Corresponding author.
E-mail: jxchen@imr.ac.cn

when the content of $Yb_4Si_2O_7N_2$ was lower than 60 vol% (or the content of *h*-BN exceeded 40 vol%), the sintering process became difficult.

Like $Y_4Si_2O_7N_2$, $Yb_4Si_2O_7N_2$ is another member of $Re_4Si_2O_7N_2$ (Re = Y and rare-earth elements) known as the J-phase, with a crystal structure of the cuspidine type ($Ca_4Si_2O_7F_2$) [22,23]. The $Yb_4Si_2O_7N_2$ phase was first found as an intergranular phase in Si_3N_4 ceramics [24]. Its formation is attributed to the following reaction [25]:

$$4Yb_2O_3 + SiO_2 + Si_3N_4 \rightarrow 2Yb_4Si_2O_7N_2 \qquad (1)$$
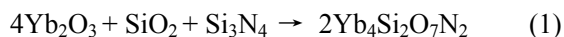
Up to now, $Yb_4Si_2O_7N_2$ has been mainly used as a refractory secondary phase to enhance the mechanical properties of Si_3N_4 ceramics, particularly the high-temperature strength [24,26–28]. It was found that Si_3N_4 ceramics could maintain a high flexural strength of 870 MPa at 1400 ℃ when $Yb_4Si_2O_7N_2$ was formed as grain boundary phase [24]. Guo *et al.* [28] studied the creep behavior of Si_3N_4 under different service temperatures and loads, and concluded that the introduction of $Yb_4Si_2O_7N_2$ favored the good creep resistance of Si_3N_4 ceramics. However, the intrinsic property of $Yb_4Si_2O_7N_2$ was rarely reported. Considering that $Yb_4Si_2O_7N_2$ phase has a slightly lower melting point (1870 ℃) than $Y_4Si_2O_7N_2$ (1880 ℃) [26], the composites containing $Yb_4Si_2O_7N_2$ may have better sinterability.

In this study, a series of *h*-BN based composites with $Yb_4Si_2O_7N_2$ as a secondary phase were synthesized by an *in situ* reaction hot pressing method. The phase compositions and microstructures were investigated. The room-temperature mechanical properties, including flexural strength, compressive strength, Vickers hardness, and fracture toughness, were measured. Significant strengthening and toughening effects were obtained, and the mechanisms were discussed.

2 Experimental procedure

The aim of this study is to fabricate easily machinable *h*-BN based composites; therefore, the upper volume fraction limit of the hard secondary phase ($Yb_4Si_2O_7N_2$) was set as 50%. The composites containing 10–50 vol% $Yb_4Si_2O_7N_2$ as a strengthening phase, abbreviated as BYb*x* (*x* = 10, 20, 30, 40, 50), were fabricated by an *in situ* reaction hot pressing method. Commercially available powders of *h*-BN (98%, 0.7 μm, Yingkou Liaobin Fine Chemical Co., Ltd., Liaoning, China), Yb_2O_3 (99.9%, 3 μm, Ganzhou Kemingrui Nonferrous

Metal Materials Co., Ltd., Jiangxi, China), SiO_2 (99%, 1 μm, Sinopharm Chemical Reagent Co., Ltd., Shanghai, China), and Si_3N_4 (99%, 1 μm, Sinopharm Chemical Reagent Co., Ltd., Shanghai, China) were used as raw materials. Table 1 lists the initial compositions for the synthesis of *h*-BN/$Yb_4Si_2O_7N_2$ composites. The powders were weighed and ball-milled in a Si_3N_4 jar with Si_3N_4 balls and ethanol as media for 12 h. After that, the obtained powders were dried, sieved, and then uniaxially compacted under 10 MPa in a graphite mold pre-sprayed with a layer of *h*-BN. The compacted mixtures were heated at a rate of 8 ℃/min under a flowing nitrogen atmosphere in a furnace using a graphite heating element. The sintering temperature was 1900–1950 ℃ with a holding time of 1.5 h, and the final applied pressure was 30 MPa.

The as-prepared sample surface was machined off in order to remove any contaminants before characterization. Phase compositions were identified by a step-scanning X-ray diffractometer (XRD, D/max-2400; Rigaku, Tokyo, Japan) with Cu Kα radiation. The microstructure was observed by a SUPRA 35 scanning electron microscope (SEM, LEO, Oberkochen, Germany) equipped with energy dispersive X-ray spectroscopy (EDX) and a 200 kV Tecnai G^2 F20 transmission electron microscope (TEM, FEI, Eindhoven, Netherlands).

The apparent density (ρ) at ambient temperature was measured by the Archimedes method. The formula for the apparent density is

$$\rho = \frac{A}{A-B}(\rho_0 - 0.0012) + 0.0012 \qquad (2)$$

where *A* is the mass of sample in air (g), *B* is the mass of sample in distilled water (g), ρ_0 is the density of distilled water at ambient temperature (g/m³), and 0.0012 is the density of air.

Theoretical density (ρ_{theo}) of the composite was calculated by formula (3), and relative density is the ratio of apparent density and theoretical density of the composite.

Table 1 Initial compositions of powders and sintering temperatures for *h*-BN/$Yb_4Si_2O_7N_2$ composites

Sample	$Yb_4Si_2O_7N_2$ content (vol%)	Compositions of powders (wt%)				Sintering temperature (℃)
		h-BN	Yb_2O_3	SiO_2	Si_3N_4	
BYb10	10	73.68	23.49	0.86	2.09	1950
BYb20	20	55.48	39.56	1.44	3.52	1950
BYb30	30	41.85	51.66	1.89	4.60	1930
BYb40	40	31.85	60.55	2.22	5.39	1930
BYb50	50	23.85	67.61	2.52	6.02	1900

$$\rho_{\text{theo}} = \rho_1 \times V_1 + \rho_2 \times V_2 \qquad (3)$$

where ρ_1 and ρ_2 are the theoretical densities of the matrix and secondary phases, respectively; V_1 and V_2 are the volume fractions of matrix and secondary phases, respectively.

Three-point bending tests were performed to measure the flexural strength (σ_F). The distance of the fixture for three-point bending test was 30 mm, and the sample size was 3 mm × 4 mm × 36 mm. The crosshead speed was 0.5 mm/min.

The fracture toughness (K_{IC}) was measured using the single-edge notched beam (SENB) method on sample with dimension of 4 mm × 8 mm × 32 mm. The notches were introduced by a diamond-coated wheel slotting. The thickness of blade was 0.15 mm, and the width of the notches was 0.2 mm. The inner and outer spans of the four-point bending test were 10 and 30 mm, respectively, and the crosshead speed was 0.05 mm/min. The testing surfaces of the samples were polished with a diamond paste of 1.5 μm to minimize the machining flaws before the bending test, and at least three samples were measured for each condition.

Compressive strength was determined by measuring seven samples with a size of 2 mm × 2 mm × 4 mm. The height of the sample was parallel to the direction of hot pressing. A crosshead speed of 0.5 mm/min was used in compressive test.

The Vickers hardness (H_V) was measured at a load of 4.9 N with dwell time of 15 s, and the given value was the average of seven separate measurements.

3   Results and discussion

3. 1   Phase compositions and microstructure

The XRD patterns of *h*-BN based composites with different volume contents of $Yb_4Si_2O_7N_2$ are shown in Fig. 1. For BYb10 and BYb20, along with the *h*-BN and $Yb_4Si_2O_7N_2$ phases, Yb_2SiO_5 is also detected. As the content of $Yb_4Si_2O_7N_2$ increases from 10 to 20 vol%, the diffraction intensity of $Yb_4Si_2O_7N_2$ increases while the intensity of Yb_2SiO_5 decreases. When the content of $Yb_4Si_2O_7N_2$ is over 30 vol%, Yb_2SiO_5 disappears and only *h*-BN and $Yb_4Si_2O_7N_2$ phases can be identified, which indicates that reaction (1) has been completed. Additionally, the diffraction intensity of *h*-BN gradually weakens as the content of $Yb_4Si_2O_7N_2$ increases from 10 to 50 vol%.

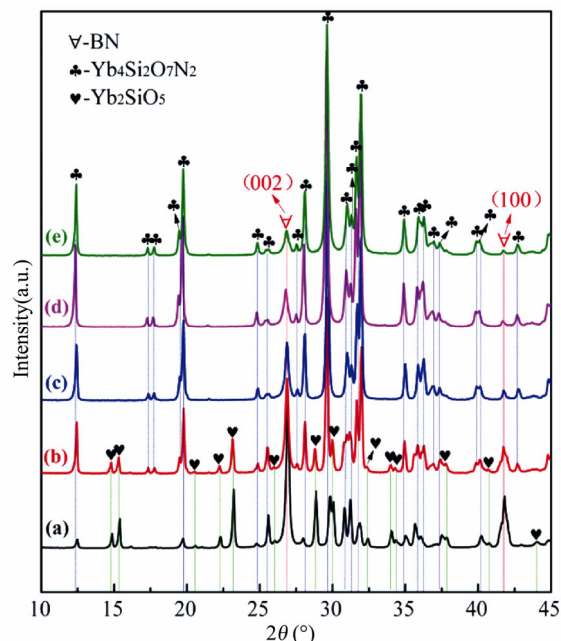**Fig. 1** XRD patterns of *h*-BN/$Yb_4Si_2O_7N_2$ composites: (a) BYb10, (b) BYb20, (c) BYb30, (d) BYb40, and (e) BYb50.

The densities of *h*-BN/$Yb_4Si_2O_7N_2$ composites are listed in Table 2. The apparent density increases from 2.15 to 4.75 g/cm^3 as the volume content of $Yb_4Si_2O_7N_2$ increases from 10% to 50%. At the same time, the relative density of the as-prepared composites increases from 77.34% to 98.75%. This means that the introduction of $Yb_4Si_2O_7N_2$ can improve the sintering ability of the composites. It is known that *h*-BN grains would grow easily along the direction perpendicular to the *c*-axis under high-temperature conditions, and the layered *h*-BN grains contact each other to form a "card bridge structure" [29]. However, when the content of the secondary phase is increased, the "card bridge structure" would be damaged, which is beneficial for the rearrangement of *h*-BN grains. Therefore, sample density increases as the content of $Yb_4Si_2O_7N_2$ increases. The increase of the relative density of the composites would be of undoubted benefit to the improvement of mechanical properties [30]. As the relative density of the BYb10 sample is too low, reliable mechanical properties could not be obtained. Therefore, the composites containing 20–50 vol% $Yb_4Si_2O_7N_2$ were mainly studied.

Table 2   Density of *h*-BN/$Yb_4Si_2O_7N_2$ composites

Composite	BYb10	BYb20	BYb30	BYb40	BYb50
Apparent density (g/cm^3)	2.15	2.82	3.58	4.14	4.75
Relative density (%)	77.34	85.71	94.21	96.28	98.75

Figure 2 shows typical backscattered electron images of polished surfaces and corresponding secondary electron morphologies of fracture surfaces of the composites containing 20 and 50 vol% $Yb_4Si_2O_7N_2$. By the result of XRD, there are *h*-BN, $Yb_4Si_2O_7N_2$, and Yb_2SiO_5 phases in the sample BYb20, but $Yb_4Si_2O_7N_2$ and Yb_2SiO_5 cannot be effectively differentiated by SEM and EDX, as shown in Fig. 2(a). The white isolate island-like secondary phases ($Yb_4Si_2O_7N_2$ and Yb_2SiO_5) distribute homogeneously throughout the black *h*-BN matrix. Furthermore, some pores can be observed on the surface. When the $Yb_4Si_2O_7N_2$ content increases to 50 vol%, continuous and interlocked distribution is obtained, as shown in Fig. 2(b).

According to the morphologies of the fracture surfaces after bending tests, *h*-BN mainly shows laminated cleavage, while $Yb_4Si_2O_7N_2$ mainly presents the transgranular fracture in sample BYb20, as shown in Fig. 2(c). However, for sample BYb50, *h*-BN shows the characteristics of laminated cleavage and transgranular fracture, and $Yb_4Si_2O_7N_2$ exhibits the transgranular and intragranular mixed fracture, as shown in Fig. 2(d). On the other hand, it can be found that the size of $Yb_4Si_2O_7N_2$ particles is approximately 1–3 μm. Because finer microstructure can be obtained when the raw powders have small particle size [31]. The particle sizes of Yb_2O_3, SiO_2, and Si_3N_4 used in this work are 3, 1, and 1 μm, respectively, and the sizes of these powders

could be smaller after ball-milled for 12 h; therefore, the reactive product $Yb_4Si_2O_7N_2$ also has finer microstructure. In addition, when more $Yb_4Si_2O_7N_2$ is introduced into the composites, which would effectively inhibit the growth of *h*-BN, so *h*-BN could also possess finer microstructure.

TEM was used to investigate the microstructure of the BYb40 composite. Figures 3(a) and 3(b) show the bright-field images. White *h*-BN grains present layered morphology, and black $Yb_4Si_2O_7N_2$ particles exist with irregular shape. Figure 3(c) is an HRTEM image of the interface indicated by the rectangle in Fig. 3(b). There are no amorphous or other impurity phases at the interface, and no micro-cracks between two phases, which demonstrates a good interfacial combination. However, due to the layered characteristic and the weak combination between layers, there are many micro-cracks in the *h*-BN grains. This phenomenon has been observed in many ceramic materials containing *h*-BN [16,29,32,33].

3. 2 Mechanical properties

The effect of the $Yb_4Si_2O_7N_2$ phase on the strength is shown in Fig. 4. The flexural strength increases by approximately 66%, from 204±12 MPa for the composite containing 20 vol% $Yb_4Si_2O_7N_2$ to 338±10 MPa for the composite containing 50 vol% $Yb_4Si_2O_7N_2$. The corresponding improvement in the compressive strength
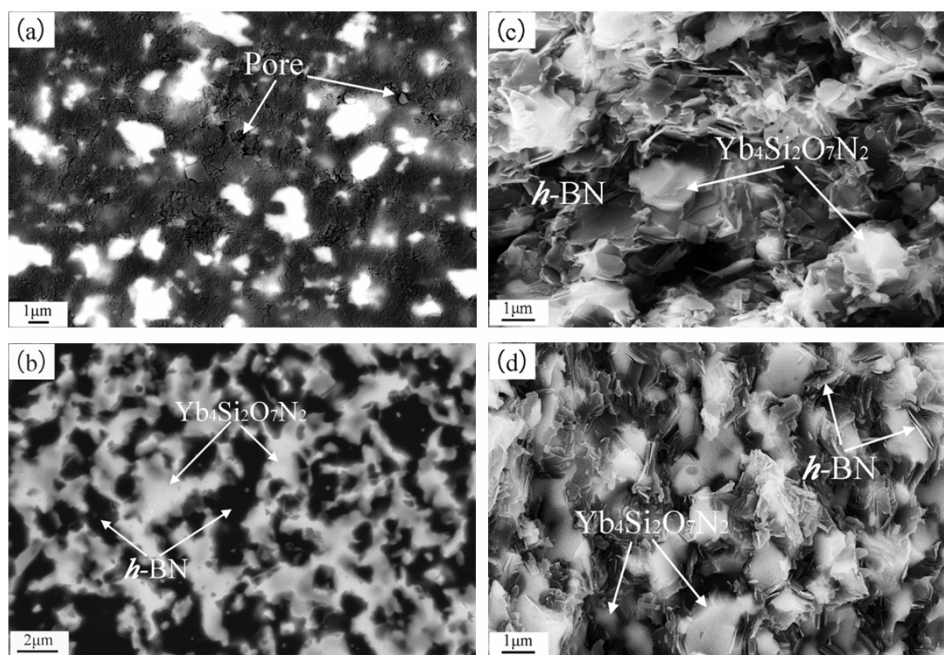

Fig. 2 Backscattered electron images of polished surfaces and secondary electron morphologies of fracture surfaces: (a, c) BYb20, (b, d) BYb50.
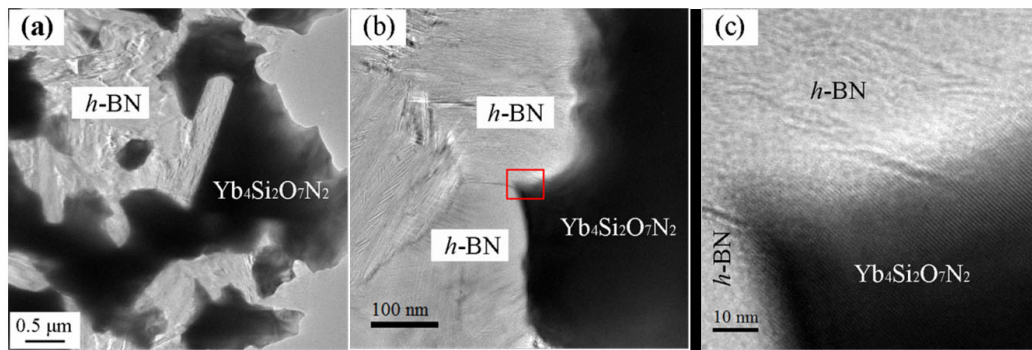
Fig. 3 TEM images of BYb40 composite: (a) bright-field image, (b) partly magnified image, and (c) HRTEM image of interface indicated by rectangle in (b).
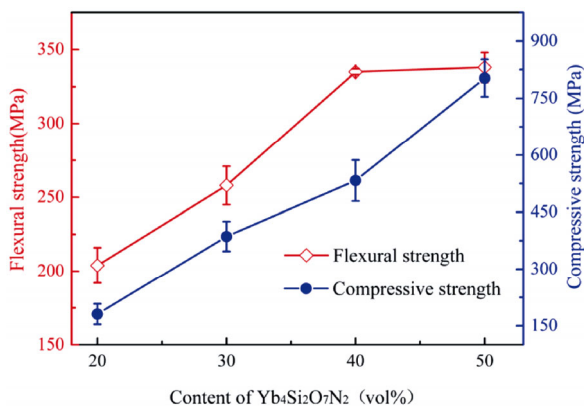

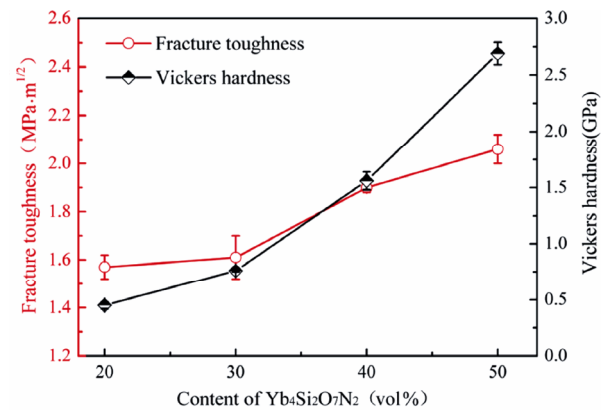**Fig. 4** Flexural strength and compressive strength of h-BN/Yb$_4$Si$_2$O$_7$N$_2$ composites.

Fig. 5 Fracture toughness and Vickers hardness of h-BN/Yb$_4$Si$_2$O$_7$N$_2$ composites.

is approximately 343%, i.e., from 181±27 to 803± 49 MPa. In particular, flexural strength is improved dramatically when the Yb$_4$Si$_2$O$_7$N$_2$ content increases from 20 to 40 vol%, and it is almost stable from 40 to 50 vol%. Meanwhile, the compressive strength of the composites tends to increase linearly. It could be seen that h-BN/Yb$_4$Si$_2$O$_7$N$_2$ composites possess higher strength than pure h-BN ceramic (75.8 MPa for flexural strength and 124.1 MPa for compressive strength) [15], and many other reported h-BN based composites, such as h-BN/Y$_2$SiO$_5$ [20], h-BN/Y$_2$Si$_2$O$_7$ [16], h-BN/SiAlON [17], and Y$_4$Si$_2$O$_7$N$_2$/h-BN [21].

Similar trends can be seen in both fracture toughness and Vickers hardness as shown in Fig. 5. The fracture toughness increases from 1.57±0.05 to 2.06±0.06 MPa·m$^{1/2}$ as the volume content of Yb$_4$Si$_2$O$_7$N$_2$ increases from 20% to 50%, while the Vickers hardness is improved dramatically. Compared to 0.45±0.03 GPa for BYb20, the value of Vickers hardness for BYb50 is 2.69±0.10 GPa.

The strengthening effect of Yb$_4$Si$_2$O$_7$N$_2$ should mainly result from its high modulus (~174 GPa) and

high hardness (~9.13±0.44 GPa), which could lead to the high deformation resistance. Coupled with the good interface combination between h-BN and Yb$_4$Si$_2$O$_7$N$_2$, the second strengthening phase can carry a load effectively. On the other hand, since the relative density increases with increasing the content of Yb$_4$Si$_2$O$_7$N$_2$ from 20 to 50 vol%, the defects should decrease consequently, and then the strengthening effect becomes significant.

In the Vickers hardness tests, no extrusion or upheaval of grains in the vicinity of indentation could be observed in all composites. However, micro-cracks exist along the direction of the indentation diagonal, which indicates that the fracture energy releases in the way of crack propagation during high applied load (49 N) on the composites. Figure 6 shows the crack propagation path of the BYb50 composite. Crack deflection and bridging could be observed as the crack followed a tortuous path. It can be seen that the crack propagates not only in the h-BN matrix but also in the Yb$_4$Si$_2$O$_7$N$_2$ phase. Additionally, the cracks could propagate along the interface between the h-BN and Yb$_4$Si$_2$O$_7$N$_2$ phases.
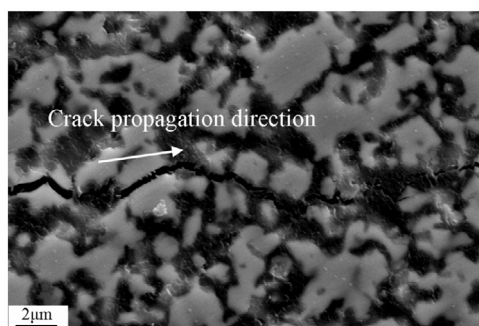
Fig. 6 Secondary electron image of crack propagation path in BYb50 composite.

Table 3 Comparison of machinability

Material	H_V (GPa)	K_{IC} (MPa·m$^{1/2}$)	H_V / K_{IC} (mm$^{-1/2}$)
BYb20	0.45	1.57	9
BYb30	0.76	1.61	15
BYb40	1.56	1.90	26
BYb50	2.69	2.06	41
BN/50 vol%Y$_2$SiO$_5$ [20]	1.50	1.57	30
BN/80 vol% Y$_4$Si$_2$O$_7$N$_2$ [32]	5.75	2.05	89
Ti$_3$SiC$_2$ [35]	4.00	7.20	18

For its high modulus and high hardness, the strengthening phase Yb$_4$Si$_2$O$_7$N$_2$ can consume more fracture energy during the processes of crack propagation. Meanwhile, the fine and even interlocked microstructure of the composites could lead to a simultaneous improvement of strength and toughness [34].

Due to the hardness of the *h*-BN/Yb$_4$Si$_2$O$_7$N$_2$ composites being relatively low (< 3 GPa), all samples obtained could be easily machined by tungsten carbide tools, which indicates that these composites maintain good machinability. As Yb$_4$Si$_2$O$_7$N$_2$ possesses a higher Vickers hardness, it is difficult to be machined. Therefore, the machinability of *h*-BN/Yb$_4$Si$_2$O$_7$N$_2$ composites results from the layered *h*-BN. The layered structure of *h*-BN is prone to interlayer splitting during machining, which can absorb a large amount of strain energy, prevent the crack's propagation, and induce composite fracture on a microscopic scale.

Table 3 lists a comparison of machinability of some materials evaluated by the value of H_V / K_{IC}. The smaller the value of H_V / K_{IC}, the better the machinability. It can be found that the value of H_V / K_{IC} becomes larger with increasing the content of Yb$_4$Si$_2$O$_7$N$_2$. However, the value of H_V / K_{IC} is only 15 mm$^{-1/2}$ when 30 vol% Yb$_4$Si$_2$O$_7$N$_2$ is introduced, which is still lower than that of one typical machinable layered ternary compound Ti$_3$SiC$_2$ [35]. Because the hardness of Yb$_4$Si$_2$O$_7$N$_2$ is higher than that of Y$_2$SiO$_5$ (5.3±0.1 GPa) [36], the composite containing 50 vol% Yb$_4$Si$_2$O$_7$N$_2$ has higher H_V / K_{IC} value compared with *h*-BN/50 vol% Y$_2$SiO$_5$ composite. Even for *h*-BN/80 vol% Y$_4$Si$_2$O$_7$N$_2$ composite, where the value of H_V / K_{IC} reaches 89 mm$^{-1/2}$, it still can be drilled by tungsten carbide tools [32]. Thus, it can be concluded that *h*-BN based composites containing 20–50 vol % Yb$_4$Si$_2$O$_7$N$_2$ have good machinability.

4　Conclusions

h-BN based composites with Yb$_4$Si$_2$O$_7$N$_2$ as the secondary phase were successfully synthesized by an *in situ* reaction hot pressing method. The incorporation of Yb$_4$Si$_2$O$_7$N$_2$ significantly improved the sinterability and room-temperature mechanical properties of the *h*-BN matrix. When 50 vol% Yb$_4$Si$_2$O$_7$N$_2$ was introduced, the relative density of the composite reached 98.75%, and its flexural strength, compressive strength, fracture toughness, and hardness reached 338±10 MPa, 803±49 MPa, 2.06± 0.06 MPa·m$^{1/2}$, and 2.69±0.10 GPa, respectively.

The strengthening mechanisms include high modulus and high hardness of Yb$_4$Si$_2$O$_7$N$_2$, the densification of the composites, and good interfacial combination between *h*-BN and Yb$_4$Si$_2$O$_7$N$_2$. Fine microstructure is also beneficial for high strength and can lead to more tortuous crack propagation paths and then improve the fracture toughness of the composites simultaneously. Additionally, *h*-BN/Yb$_4$Si$_2$O$_7$N$_2$ composites have good machinability, which is attributed to their low hardness and improved fracture toughness.

References

[1] Sinclair W, Simmons H. Microstructure and thermal shock behaviour of BN composites. *J Mater Sci Lett* 1987, **6**: 627–629.

[2] Lipp A, Schwetz KA, Hunold K. Hexagonal boron nitride: Fabrication, properties and applications. *J Eur Ceram Soc* 1989, **5**: 3–9.

[3] Zhang G-J, Yang J-F, Ohji T, *et al.* In-situ reaction synthesis of non-oxide boron nitride composites. *Adv Eng Mater* 2002, **4**: 15–17.

[4] Eichler J, Lesniak C. Boron nitride (BN) and BN composites for high-temperature applications. *J Eur Ceram Soc* 2008, **28**: 1105–1109.

[5] Zhang X, Zhang R, Chen G, *et al.* Microstructure, mechanical properties and thermal shock resistance of hot-pressed $ZrO_2(3Y)$–BN composites. *Mat Sci Eng A* 2008, **497**: 195–199.

[6] Liang F, Xue Z, Zhao L, *et al.* Mechanical properties and thermal shock resistance of alumina/hexagonal boron nitride composite refractories. *Metall and Mat Trans A* 2015, **46**: 4335–4341.

[7] Rusanova LN, Romashln AG, Kullkova GI, *et al.* Boron nitride ceramics: Problems and development perspectives. *Powder Metall Met Ceram* 1988, **27**: 21–28.

[8] Zhang G-J, Yang J-F, Andoa M, *et al.* Nonoxide-boron nitride composites: in situ synthesis, microstructure and properties. *J Eur Ceram Soc* 2002, **22**: 2551–2554.

[9] Haubner R, Wilhelm M, Weissenbacher R, *et al.* Boron nitrides—Properties, synthesis and applications. In: *High Performance Non-Oxide Ceramics II. Structure and Bonding, Vol. 102*. Jansen M, Ed. Springer Berlin Heidelberg, 2002: 1–45.

[10] Li Y, Wu H, Yin J, *et al.* High electrical resistivity of pressureless sintered in situ SiC–BN composites. *Scripta Mater* 2013, **69**: 740–743.

[11] Frederikse HPR, Kahn AH, Dargoo AL, *et al.* Electrical resistivity and microwave transmission of hexagonal boron nitride. *J Am Ceram Soc* 1985, **68**: 131–135.

[12] Jin H-Y, Xu H, Qiao G-J, *et al.* Study of machinable silicon carbide–boron nitride ceramic composites. *Mat Sci Eng A* 2008, **483–484**: 214–217.

[13] Zhong B, Zhao GL, Huang XX, *et al.* Microstructure and mechanical properties of ZTA/BN machinable ceramics fabricated by reactive hot pressing. *J Eur Ceram Soc* 2015, **35**: 641–649.

[14] Li Y, Yin J, Wu H, *et al.* Enhanced electrical resistivity in SiC–BN composites with highly-active BN nanoparticles synthesized via chemical route. *J Eur Ceram Soc* 2015, **35**: 1647–1652.

[15] MatWeb, The online materials database, GE advanced ceramics HBN hot-pressed boron nitride. Available at http://www.matweb.com/search/datasheet.aspx?matguid=8 fbbb7d47809493e9afbb7778657d5bb.

[16] Trice RW, Halloran JW. Investigation of the physical and mechanical properties of hot-pressed boron nitride/oxide ceramic composites. *J Am Ceram Soc* 1999, **82**: 2563–2565.

[17] Tian Z, Jia DC, Duan XM, *et al.* Effects of AlN content on phase composition, microstructure and mechanical properties of BN-based composite ceramics. *J Chin Ceram*

[18] *Soc* 2013, **41**: 1603–1608. (in Chinese)

[18] Zhang X. Preparation and properties of rare earth silicate (RE_2SiO_5, $RE_2Si_2O_7$, RE = Y, Yb) modified boron nitride matrix composites. Ph.D. Thesis. Shenyang, China: Institute of Metal Research, Chinese Academy of Sciences, 2015. (in Chinese)

[19] Zhang X, Chen J, Zhang J, *et al.* High-temperature mechanical and thermal properties of *h*-BN/30 vol%Y_2SiO_5 composite. *Ceram Int* 2015, **41**: 10891–10896.

[20] Zhang X, Chen J, Li X, *et al.* Microstructure and mechanical properties of *h*-BN/Y_2SiO_5 composites. *Ceram Int* 2015, **41**: 1279–1283.

[21] Chen L, Chen JX. Thermal shock resistance of $Y_4Si_2O_7N_2$–BN composites. *J Henan Normal Univ: Nat Sci Ed* 2011, **39**: 70–72. (in Chinese)

[22] Takahashi J, Yamane H, Shimada M, *et al.* Crystal structure of $Lu_4Si_2O_7N_2$ analyzed by the Rietveld method using the time-of-flight neutron powder diffraction pattern. *J Am Ceram Soc* 2002, **85**: 2072–2077.

[23] Takahashi J, Yamane H, Hirosaki N, *et al.* Crystal structure of rare-earth silicon-oxynitride J-phases, $Ln_4Si_2O_7N_2$. *J Eur Ceram Soc* 2005, **25**: 793–799.

[24] Park H, Kim H-E, Niihara K. Microstructural evolution and mechanical properties of Si_3N_4 with Yb_2O_3 as a sintering additive. *J Am Ceram Soc* 1997, **80**: 750–756.

[25] Nishimura T, Mitomo M. Phase relationships in the system Si_3N_4–SiO_2–Yb_2O_3. *J Mater Res* 1995, **10**: 240–242.

[26] Nishimura T, Mitomo M, Suematsu H. High temperature strength of silicon nitride ceramics with ytterbium silicon oxynitride. *J Mater Res* 1997, **12**: 203–209.

[27] Lu H-H, Huang J-L. Effect of Y_2O_3 and Yb_2O_3 on the microstructure and mechanical properties of silicon nitride. *Ceram Int* 2001, **27**: 621–628.

[28] Guo S, Hirosaki N, Nishimura T, *et al.* Compressive creep behaviour of $Yb_4Si_2O_7N_2$ containing silicon nitride ceramic between 1400 and 1500 ℃. *Mater Sci Technol* 2003, **19**: 544–548.

[29] Wen G, Wu GL, Lei TQ, *et al.* Co-enhanced SiO_2–BN ceramics for high-temperature dielectric applications. *J Eur Ceram Soc* 2000, **20**: 1923–1928.

[30] Coble RL, Kingery WD. Effect of porosity on physical properties of sintered alumina. *J Am Ceram Soc* 1956, **39**: 377–385.

[31] Özcan S, Açıkbaş G, Özbay N, *et al.* The effect of silicon nitride powder characteristics on SiAlON microstructures, densification and phase assemblage. *Ceram Int* 2017, **43**: 10057–10065.

[32] Chen L. Synthesis, microstructure, and properties of $Y_4Si_2O_7N_2$–BN composites. M.Sc. Thesis. Shenyang, China: Institute of Metal Research, Chinese Academy of Sciences, 2011. (in Chinese)

[33] Duan X, Jia D, Zhou Y, *et al.* Mechanical properties and

plasma erosion resistance of BNp/Al$_2$O$_3$–SiO$_2$ composite ceramics. *J Cent South Univ* 2013, **20**: 1462–1468.

[34] Calis Acikbas N, Kumar R, Kara F, *et al*. Influence of β-Si$_3$N$_4$ particle size and heat treatment on microstructural evolution of α:β-SiAlON ceramics. *J Eur Ceram Soc* 2011, **31**: 629–635.

[35] Li S, Xie J, Zhao J, *et al*. Mechanical properties and mechanism of damage tolerance for Ti$_3$SiC$_2$. *Mater Lett* 2002, **57**: 119–123.

[36] Sun Z, Wang J, Li M, *et al*. Mechanical properties and damage tolerance of Y$_2$SiO$_5$. *J Eur Ceram Soc* 2008, **28**: 2895–2901.